Atmos. Chem. Phys., 26, 4439–4451, 2026
https://doi.org/10.5194/acp-26-4439-2026

Atmospheric Chemistry and Physics
Open Access
EGU

Research article

The effect of organic nucleation on the indirect radiative forcing with a semi-explicit chemical mechanism for highly oxygenated organic molecules (HOMs)

Xinyue Shao[1,2,3,4,5], Minghuai Wang[1,2,3], Xinyi Dong[2,3,4,5], Yaman Liu[3,6], Stephen R. Arnold[5], Leighton A. Regayre[5,6,7], Duseong S. Jo[8], Wenxiang Shen[1,2], Hao Wang[1,2], Man Yue[1,4], Jingyi Wang[1,2], Wenxin Zhang[1,2], and Ken S. Carslaw[5]

[1]State Key Laboratory of Severe Weather Meteorological Science and Technology, Nanjing University, Nanjing, China
[2]Joint International Research Laboratory of Atmospheric and Earth System Sciences, Nanjing University, Nanjing, China
[3]School of Atmospheric Sciences, Nanjing University, Nanjing, China
[4]Frontiers Science Center for Critical Earth Material Cycling, Nanjing University, Nanjing, China
[5]Jiangsu Provincial Collaborative Innovation Center of Climate Change, Nanjing, China
[6]Zhejiang Institute of Meteorological Sciences, Hangzhou, China
[7]Centre for Environmental Modelling and Computation, School of Earth and Environment, University of Leeds, Leeds, LS2 9JT, UK
[8]Department of Earth Science Education, Seoul National University, Seoul, 08826, South Korea

Correspondence: Minghuai Wang (minghuai.wang@nju.edu.cn) and Xinyi Dong (dongxy@nju.edu.cn)

Received: 26 December 2024 – Discussion started: 3 February 2025
Revised: 15 July 2025 – Accepted: 5 August 2025 – Published: 1 April 2026

Abstract. Highly oxygenated organic molecules (HOMs) can significantly contribute to new particle formation (NPF). HOM-derived NPF in preindustrial (PI) environments provides the baseline for calculating radiative forcing, yet global model studies examining this are lacking. Here, we use a global climate model with a semi-explicit HOM chemistry and the associated nucleation scheme to systematically quantify the effect of HOM-derived NPF on cloud condensation nuclei (CCN) formation and effective radiative forcing due to aerosol–cloud interactions (ERF_{aci}). The model shows better agreement with measured CCN numbers after including organic NPF mechanisms. Aerosols generated from organic NPF nearly double the globally averaged CCN burden in PI (39 %) compared to present-day (PD) (18 %) experiments. This weakens the ERF_{aci} by 0.4 W m^{-2}, corresponding to a 16 % reduction, with most of this reduction occurring in tropical regions where the pure organic nucleation rate shows a larger value in the PI atmosphere. The reduction is mainly driven by a greater enhancement of the sub-20 nm growth rate (GR) in the PI atmosphere compared to PD, in contrast to the findings of Gordon et al. (2016) that the $\sim$ 1 nm nucleation rate ($j_{1.7\,nm}$) drives the reduction. The greater enhancement of GR is due to higher HOM concentrations in the PI atmosphere, while the greater $j_{1.7\,nm}$ in the PD environment results from higher sulfuric acid concentrations, leading to higher heteromolecular nucleation rates involving sulfuric acid and organics. The significant reduction underscores the critical role of biogenic NPF in CCN formation, particularly in the PI climate when cloud droplet concentrations and albedo are more sensitive to aerosol changes.

Published by Copernicus Publications on behalf of the European Geosciences Union.

1 Introduction

Atmospheric aerosols can affect climate indirectly by acting as cloud condensation nuclei (CCN), which modify cloud properties and precipitation (Rosenfeld and Lensky, 1998; Rosenfeld and Woodley, 2000; Twomey, 1977; Albrecht, 1989). The effective radiative forcing due to aerosol–cloud interactions (ERF_{aci}) remains one of the largest uncertainties in interpreting climate change over the past century and projecting future changes (Watson-Parris and Smith, 2022; Peace et al., 2020). Atmospheric new particle formation (NPF) is the largest source of atmospheric aerosol number concentrations (Gordon et al., 2017; Lee et al., 2019) and is thought to contribute up to half of the global cloud condensation nuclei (CCN) number (Spracklen et al., 2008; Merikanto et al., 2009; Williamson et al., 2019). Global climate model simulations indicate that aerosol ERF_{aci} is sensitive to parameterisations of NPF processes (Wang and Penner, 2009; Kazil et al., 2010; Gordon et al., 2017; Zhu et al., 2019; Yu et al., 2012).

Recent studies have highlighted the significant role of monoterpene-derived highly oxygenated organic molecules (HOMs) in NPF processes and their potential impact on regulating CCN concentrations, even in the absence of sulfuric acid. Ehn et al. (2014) found significant contributions of HOMs to the growth of particles ranging from 5 to 50 nm in diameter in boreal forests. Jokinen et al. (2015) showed that monoterpene-derived HOMs facilitate NPF and growth in continental regions, especially under conditions of high supersaturation, favourably affecting the concentration of CCN using chamber experiments. Using the regional model WRF-Chem, Zhao et al. (2020) showed that in the Amazon region, biogenic HOMs predominantly lead to the formation of new particles at altitudes of 13 km, in a location minimally influenced by human activities, thereby making a significant contribution to CCN formation (Zhao et al., 2022). Similarly, Wang et al. (2023) analysed the sources of aerosols in the Amazonian boundary layer using the HadGEM3 climate model, incorporating the biogenic nucleation mechanism along with its precursor gas (HOMs) from the parameterisation in Gordon et al. (2016).

Although HOMs are important for NPF due to their low volatility, their chemical formation pathways remain uncertain, and they are treated in various simplified ways in models. Gordon et al. (2016) simulated monoterpene-derived HOM formation using a fixed yield of HOMs from first-stage monoterpene oxidation products. Zhu et al. (2019) added some explicit chemical mechanisms for HOMs, but they did not consider autoxidation and used a less rigorous definition of HOMs than recommended in Bianchi et al. (2019). Also, they did not account for organic nucleating species oxidised from isoprene. Therefore, the contribution of accretion products (ACCs) generated from cross-reactions of isoprene- and monoterpene-derived radicals was significantly underestimated. Roldin et al. (2019) and Weber et al. (2020) employed more explicit reaction mechanisms to treat the generation of HOMs through autoxidation and cross-reactions of α-pinene oxidation products, but neither applied these chemical mechanisms on a global scale. Xu et al. (2022) summarised various chemical mechanisms of HOMs, including monoterpene-derived peroxy radical (MT-RO_2) unimolecular autoxidation and self- and cross-reactions with other RO_2 species, in the GEOS-Chem global model but did not consider their role in the NPF process.

HOM-driven NPF is likely to be particularly important in the pristine preindustrial (PI) atmosphere, where concentrations of sulfuric acid and ammonia were much lower. Simulations of the preindustrial atmosphere form the baseline for calculations of anthropogenic radiative forcing in global models (Carslaw et al., 2013), where higher monoterpene emissions led to greater HOM concentrations, thereby enhancing nucleation and particle growth. Using global model simulations, Gordon et al. (2016) showed that new particles formed from monoterpene-derived HOMs could increase CCN concentrations in the PI environment by 20 % to 100 %, a rise considerably larger than the increase simulated for present-day (PD) conditions. This increase led to a 27 % reduction in negative radiative forcing since 1750, decreasing by between -0.28 and $-0.06\,W\,m^{-2}$. Similarly, Zhu et al. (2019), utilising simulations with the Community Earth System Model (CESM), found that new particles formed from monoterpene-derived HOMs have reduced the direct plus indirect radiative forcing of aerosols by 12.5 % since the Industrial Revolution. However, they did not use explicit chemical processes to represent HOM chemistry, potentially leading to inaccuracies in the PI and present-day (PD) simulations for radiative forcing calculations due to anthropogenic emissions. The uncertainty in this baseline is one of the largest components of the overall uncertainty in aerosol radiative forcing (Seinfeld et al., 2016; Carslaw et al., 2013).

Considering the unequivocal evidence for the role of biogenic organics in producing atmospheric particles, Shao et al. (2024) recently incorporated a state-of-the-art representation of HOMs from various chamber experiments (Xu et al., 2022). This representation semi-explicitly treats the unimolecular autoxidation of monoterpene-derived RO_2 radicals and their self- and cross-reactions with other RO_2 species, rather than using the empirical fixed HOM yield. In addition, Shao et al. (2024) introduced a HOM-involving nucleation parameterisation (Riccobono et al., 2014; Kirkby et al., 2016) and enabled these organics to condense onto newly formed sub-20 nm particles. The updated model demonstrates significant improvements in simulating NPF events and aerosol number concentrations, showing better agreement with measurements (Shao et al., 2024). Here, we seek to estimate the change in ERF_{aci} resulting from the inclusion of organic particle formation based on this model and highlight the key processes driving this change.

The model and field measurements used in this study are documented in Sect. 2. Section 3 evaluates CCN number concentrations in the updated model. Section 4 quantifies the contributions of organic NPF to CCN number globally in both present-day (PD) and PI environments. The change in effective radiative forcing due to aerosol–cloud interactions (ERF_{aci}) associated with organic NPF processes is also calculated. Results are summarised and discussed in Sect. 5.

2 Data and methods

2.1 Model configuration

In this study, we examine the impact of organic NPF on atmospheric aerosols and the Earth's radiative balance using the atmospheric module of the Community Earth System Model (CESM) version 2.1.0, specifically the Community Atmosphere Model version 6, which is enhanced with extensive tropospheric and stratospheric chemistry (CAM6-Chem) (Emmons et al., 2020). The model uses the MOZART-TS2 gas-phase chemistry scheme (Schwantes et al., 2020) and employs a four-mode version of the Modal Aerosol Module (MAM4) (Liu et al., 2016). The default configuration of CAM6-Chem includes binary homogeneous nucleation of H_2SO_4–H_2O (Vehkamaki et al., 2002) and ternary homogeneous nucleation of H_2SO_4–NH_3–H_2O (Merikanto et al., 2007). Additionally, within the boundary layer, the model includes the empirical nucleation mechanism (Kulmala et al., 2006; Sihto et al., 2006).

Our previous study (Shao et al., 2024) incorporated the representation of HOM chemistry from Xu et al. (2022) (including monoterpene-derived peroxy radical (MT-RO_2) unimolecular autoxidation and self- and cross-reactions with other RO_2 species). In total, 24 reactions in CAM6-Chem were modified and 96 reactions were added to more explicitly simulate HOM chemistry (Sect. S1). Shao et al. (2024) also updated inorganic nucleation rates involving H_2SO_4 and NH_3 as well as ion-induced pathways based on the CLOUD chamber experiments (Dunne et al., 2016), replacing the default scheme based on H_2SO_4 and NH_3 (Vehkamaki et al., 2002; Merikanto et al., 2007). The organic nucleation scheme was also added in CAM6-Chem, including heteromolecular nucleation of sulfuric acid and organics ($J_{SA\text{-}Org}$) (Riccobono et al., 2014), neutral pure organic nucleation ($J_{Org,n}$), and ion-induced pure organic nucleation ($J_{Org,i}$) (Kirkby et al., 2016). Organic vapour condensation on newly formed particles was also added in our updated model (Eq. 12 in Shao et al., 2024).

The abovementioned updated nucleation rate and sub-20 nm particle growth rates have already been evaluated in our previous study (Shao et al., 2024), in better agreement with observations at numerous sites. Therefore, the performance of NPF event frequency and N10 (number concentrations for particles with diameters larger than 10 nm) also shows reasonable agreement with measurements (Shao et al., 2024).

2.2 Case setting

We calculated the ERF_{aci} between preindustrial (PI) and present-day (PD) cases using the methodology from Ghan (2013). The effect of biogenic organic NPF on the magnitude of ERF_{aci} was calculated by comparing simulations with (using Eqs. 2–8 in Shao et al., 2024, named "Inorg_Org" in Table 1) and without (using only Eqs. 6–8 in Shao et al., 2024, named "Inorg" in Table 1) biogenic NPF mechanisms. The prefixes "PD" and "PI" in each test name represent emissions scenarios appropriate for the present-day and preindustrial periods (Table 1).

Ten-year simulations were performed with $0.9° \times 1.25°$ spatial resolution and a vertical resolution extending up to approximately 40 km across 32 layers (Emmons et al., 2020) for both present-day (PD) and preindustrial (PI) atmospheres with an additional 1-year spin-up period (Table 1). Sea surface temperature and sea-ice extents were prescribed to climatological values for the year 2000 in both PD and PI cases. Anthropogenic and monthly biomass burning emissions were provided by the Community Emission Data System (CEDS v2017-05-18) (Hoesly et al., 2018) and the historical global biomass burning emissions inventory (van Marle et al., 2017) developed for CMIP6. For PD simulation, emissions after 2014 followed the SSP585 scenario, based on the Shared Socioeconomic Pathway 5 (SSP5) (O'Neill et al., 2017). Biogenic emissions were dynamically simulated using the Model of Emissions of Gases and Aerosol from Nature version 2.1 (MEGAN2.1) (Guenther et al., 2012). The Multi-resolution Emission Inventory for China (MEIC) (http://www.meicmodel.org, last access: 20 December 2025) (Li et al., 2017; Yue et al., 2023) was used to replace the CMIP6 emission inventory for China, as CMIP6 underestimates the reduction of SO_2 emissions after 2007.

In order to compare simulated CCN with measurements, several short-term simulations were performed, in which meteorological fields (temperature and wind profiles, surface pressure, surface stress, surface heat, and moisture fluxes) were nudged toward Modern-Era Retrospective analysis for Research and Applications (MERRA2) reanalysis with a relaxation timescale of 6 h (Kooperman et al., 2012). The simulation period corresponded to the time of measurements (Table 2), with an additional month for spin-up. Meteorological fields were nudged towards MERRA2 every 0.5 h, which is the same as the physics time step of the model. The simulated meteorological fields and their deviations from the MERRA2 reanalysis are presented in Fig. S20.

Table 1. Configurations of CESM2.1.0 experiments (long-term simulation).

Test name	Simulation period	Spin-up	Updated inorganic nucleation	HOM chemistry	Organic nucleation and growth
Inorg	corresponds to the measurements in Table 2	1 month	✓	✓	×
Inorg_Org			✓	✓	✓
PD_Inorg	Jan 2008–Dec 2017	1 year (Jan 2007–Dec 2007)	✓	✓	×
PD_Inorg_Org			✓	✓	✓
PI_Inorg	Jan 1851–Dec 1860	1 year (Jan 1850–Dec 1850)	✓	✓	×
PI_Inorg_Org			✓	✓	✓

2.3 Observation data

In our previous study (Shao et al., 2024), we evaluated NPF-related variables, including the nucleation rate, growth rate, NPF frequency, condensation sink, and aerosol number concentration in the updated model. Here, we focus specifically on evaluating the CCN number concentration in both Inorg_Org and Inorg models. The CCN number concentration is crucial because it influences the degree of cooling of the Earth's surface through the aerosol–cloud interaction, specifically by influencing cloud albedo and cloud lifetime (Twomey, 1977; Albrecht, 1989).

The observational data of CCN number concentrations used in this study were obtained from ships, stations, and aircraft at various locations (see Table 2) (Jefferson, 2010; Uin et al., 2019; Bodhaine, 1983; Wang et al., 2022; Wood et al., 2015; Zheng et al., 2020) (all the data are available for download at http://www.archive.arm.gov/discovery/#v/results/, last access: 20 December 2025). All data were processed within the Global Aerosol Synthesis and Science Project (GASSP) (Reddington et al., 2017). The CCN number measurements exhibit a very high temporal resolution (< 1 min). However, the model output's physical time step is only half an hour, making it impossible to precisely match the observation data with the model output. Consequently, we selected CCN number concentrations at supersaturations (ss) of 0.1 %, 0.2 %, 0.5 %, and 1 % from the observational data to represent different atmospheric supersaturations. These values were then compared with the model's monthly average output at the same supersaturation levels for the corresponding time period (Fig. 1).

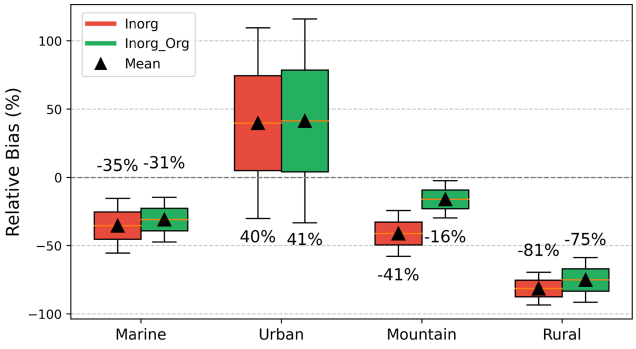

Figure 1. Box plots showing the relative bias (%) between simulated monthly mean and observed median CCN number concentrations across categorised background sites (Marine, Urban, Mountain, Rural). Red and green boxes represent the Inorg and Inorg_Org experiments, respectively. Black triangles indicate the mean relative bias for each category. Numerical values above the boxes denote the corresponding mean normalised mean bias (NMB) for each experiment. Information on the measurement sites is provided in Table 2.

3 Evaluation of simulated CCN concentrations

The underestimation of CCN numbers in the Inorg simulation is alleviated by incorporating organic-related NPF, especially over rural and mountainous regions (Fig. 1), where both nucleation and initial growth rates are dominated by biogenic pathways. The remaining underestimation of CCN in rural regions (Fig. 1) is likely due to the neglect of anthropogenic-derived HOMs, which may play a key role in NPF in these areas. The increase in CCN number due to the addition of organic NPF mechanisms is simulated not only in the locations listed in Table 2 but also on a global scale (see Fig. 7). In urban regions, the overestimation of CCN numbers is exacerbated (Fig. 1). These overestimations in CCN numbers in the Inorg model are likely related to the overestimation of H_2SO_4 concentration in CAM6-Chem (Shao et al., 2024), as these regions are more sensitive to sulfuric acid due to the limited presence of organic NPF precursors like monoterpenes. The overestimation of H_2SO_4 concentrations in the CAM-Chem model is likely the result of multiple contributing factors, such as overestimated SO_2 emissions (He and Zhang, 2014), insufficient representation of in-cloud chemistry (Ge et al., 2021, 2022), and underestimated wet deposition processes (He et al., 2015; He and Zhang, 2014). Overall, the relative bias of CCN numbers at different supersaturation levels decreases from −57 % (Inorg) to −45 % (Inorg_Org) (Fig. S18), indicating that the Inorg_Org model provides a more accurate representation of organic contributions for further quantification in Sect. 3.

Table 2. Field measurements used in this study.

Station	Type	Altitude (m a.s.l.)	Latitude	Longitude	Time
Barrow, Alaska, USA	Marine	8.0	71.32° N	156.61° W	Jan 2008–Jan 2013
Eastern North Atlantic	Marine	26.0	39.09° N	28.03° W	Nov 2014–Apr 2015
Graciosa Island	Marine	26.0	39.09° N	28.03° W	May 2009–Nov 2010
Manacapuru, Brazil	Urban	50.0	−3.21° S	60.60° W	Feb 2014–May 2015
Nainital, India	Mountain	1936.0	29.36° N	79.46° E	Jun 2011–Mar 2012
Shouxian, China	Rural	22.7	32.56° N	116.78° E	May 2008–Oct 2008
Steamboat Springs, USA	Mountain	2440.0	40.45° N	106.79° W	Oct 2010–Apr 2011
Chilbolton, UK	Rural	80.0	51.15° N	1.44° W	Feb–Mar 2009

4 Results

4.1 Change in CCN and cloud droplet number concentrations

The inclusion of organic NPF results in a greater increase in the CCN burden in the PI experiment (∼ 39 %) compared to the PD experiment (∼ 18 %) (Fig. 2). The spatial pattern of change in CCN burden (Fig. 2) is consistent with the change in aerosol burden in the Aitken and accumulation mode (Figs. S11 and S12) but affects much wider areas. Because ultrafine particles (< 50 nm) are quickly lost by coagulation to larger, pre-existing aerosol, CCN typically have a longer atmospheric lifetime and are less efficiently removed than smaller aerosol particles, allowing them to exert influence over wider spatial scales (Pierce and Adams, 2009). On the western side of the Amazon basin, the highest rise (> 50 %) in both PD and PI experiments is caused by high CCN burden transported from the Amazon basin. Such a significant change in CCN production across the unpolluted PI atmosphere is particularly important for global climate because cloud droplet number concentrations (CDNCs) are sensitive to CCN changes. Therefore, CDNCs at the top of low clouds in Inorg_Org rise by 12 % in the PI experiments but only by 7 % in the PD experiments compared to Inorg (Fig. 3).

In both the PD and PI experiments, the largest increase in CCN burden (> 20 % rise in Inorg_Org compared to Inorg) is found in the tropical regions (Amazon, central Africa, and Southeast Asia) (Fig. 2). This is attributed to the highest biogenic emissions (Fig. S3), which lead to the greatest increases in both nucleation and growth rates in Inorg_Org (Fig. 4) and the originally low aerosol number before adding organic NPF (i.e. Inorg simulation) in these regions. The enhancement in nucleation rates due to the inclusion of organic nucleation is more significant in the PD experiment (39 %) compared to the PI experiment (6 %) (Fig. 4). This is mainly caused by higher sulfuric acid concentrations in the PD environment (Fig. S2), resulting in higher heteromolecular nucleation rates involving sulfuric acid and organics (Figs. S6 and S7) over land, where both H_2SO_4 and HOMs show high values. Consequently, more H_2SO_4 is consumed over land (Fig. S16), reducing its transport to oceanic regions (Fig. S17). As a result, nucleation rates decrease over the ocean in both PD and PI experiments (Fig. 4). In contrast to organic nucleation, the impact of the organic growth rate on the total growth rate is more significant in the PI atmosphere, reaching 83 %, while in the PD atmosphere, this impact is only 23 %. This is mainly due to significantly higher emissions of organic precursors, such as monoterpenes and isoprene in the PI atmosphere (Fig. S3), and the organic growth rate is influenced only by the HOM concentrations. Therefore, compared to the increase in the ∼ 1.7 nm nucleation rate, the increase in the sub-20 nm growth rate plays a more significant role in greater increase of CCN burden in the PI experiment (Figs. 4 and S13). The strong correlation ($R \sim 0.7$) between organic growth rates and CCN burden (Fig. S15), along with the lack of substantial changes in other components of the CCN budget (Table S5), further supports this point.

4.2 Effect on aerosol indirect radiative forcing

The significant increase in CCN burden (Fig. 2) and CDNC (Fig. 3) in the PI experiment resulting from the inclusion of the organic NPF scheme is likely to reduce the aerosol radiative forcing. Thus, in this study, we focus on quantifying the effect of including biogenic organic NPF on the indirect aerosol forcing component (ERF_{aci}). The effect of organic NPF on the magnitude of ERF_{aci} is calculated by comparing simulations with (Inorg_Org) and without (Inorg) organic nucleation and growth mechanisms. To analyse the change in ERF_{aci}, we also compare the fractional changes of other key variables (nucleation rate, growth rate, aerosol number, CCN number, and CDNC) from PI to PD in Inorg_Org and Inorg (Fig. 7).

We estimate that the global ERF_{aci} since 1850, after including organic NPF, is $-2.18\,W\,m^{-2}$ (Fig. 6a). The calculated aerosol ERF_{aci} decreases by approximately $0.4\,W\,m^{-2}$ (corresponding to a 16 % reduction) after adding organic NPF mechanisms (Fig. 6b). The global mean effective radiative forcing due to aerosol–radiation interactions (ERF_{ari}) changes only slightly, from 0.03 to $-0.01\,W\,m^{-2}$, a negligible change compared to the total aerosol radiative forcing,

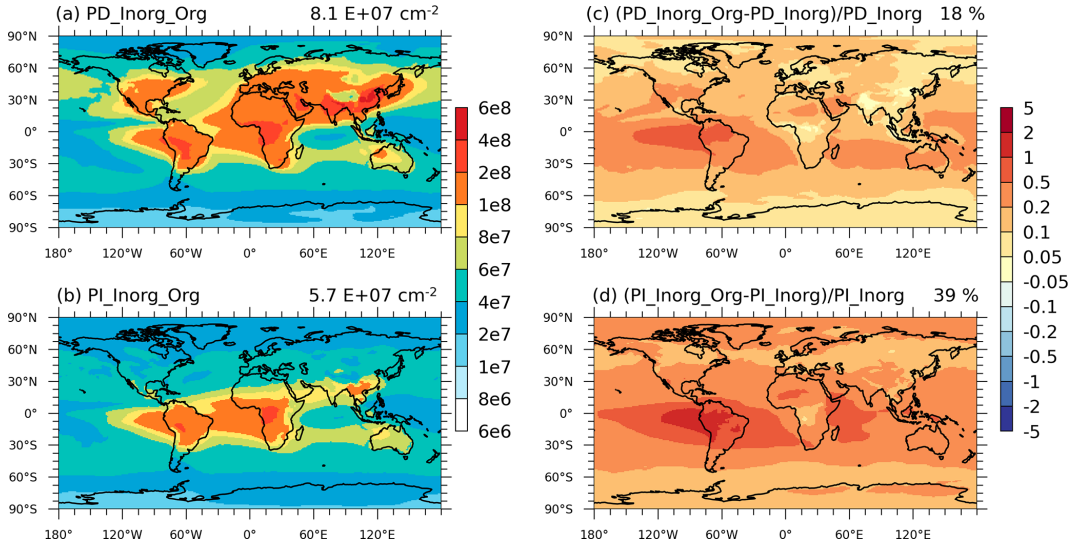

Figure 2. Spatial distribution of the simulated vertically integrated CCN at 0.2 % supersaturation (ss) in **(a)** PD_Inorg_Org and **(b)** PI_Inorg_Org (unit: cm^{-2}). The relative change after adding organic NPF in PD and PI environments is shown in **(c)** and **(d)**. Global mean values are shown on the top right of each figure.

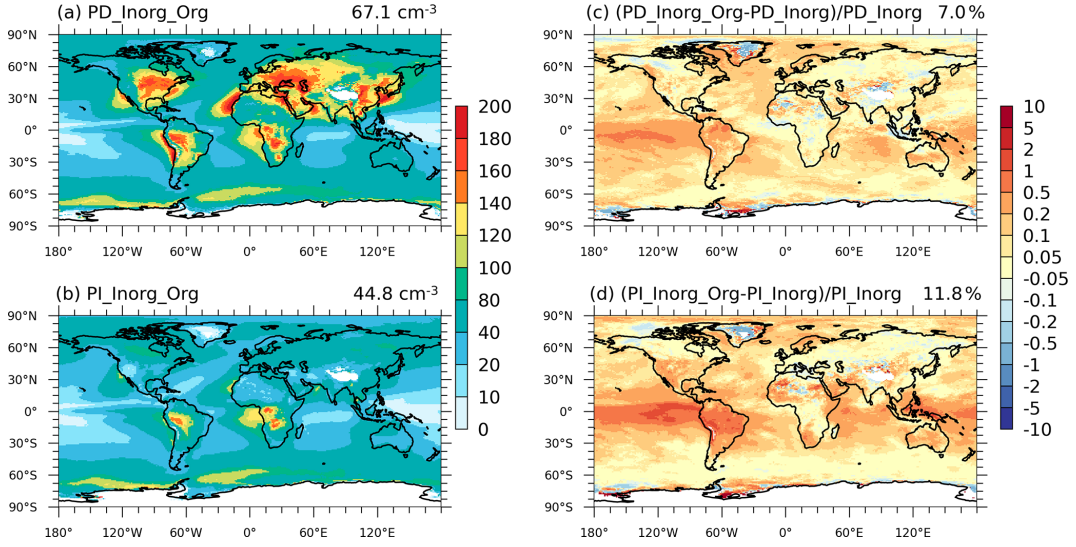

Figure 3. Spatial distribution of the simulated cloud droplet number concentration (CDNC) at the top of low clouds in **(a)** PD_Inorg_ Org and **(b)** PI_Inorg_Org (unit: cm^{-3}). The relative change after adding organic NPF in PD and PI environments is shown in **(c)** and **(d)**. Global mean values are shown on the top right of each figure.

which decreases from -2.19 to $-2.64\,W\,m^{-2}$ (Table S4). This reduction is attributed to the greater increase in CCN number in the PI experiment compared to the PD experiment (Fig. 2) when adding organic NPF (Inorg_Org), leading to a smaller relative difference in these variables between the PD and PI experiments (66 % in Inorg_Org and 41 % in Inorg; Fig. 7).

The largest reduction in ERF_{aci} occurs over the tropical region (-35 to 35° N) (Fig. 6c), especially over oceans with high low cloud cover, such as the western side of the Amazon basin and eastern China (Fig. 6b). This corresponds to the change in the CCN number and CDNC in the PI experiments, which also shows the largest increase in tropical regions. The average ERF_{aci} decreases by approximately $1\,W\,m^{-2}$ between 35° S and 35° N, with a more significant effect in the Northern Hemisphere (NH) (Fig. 6b and c). This is mainly attributed to the largest reduction in the PD fractional change of the vertically integrated CCN number in the northern United States, southeastern United States, and India in Inorg_Org compared to Inorg (Fig. 5b). These signif-

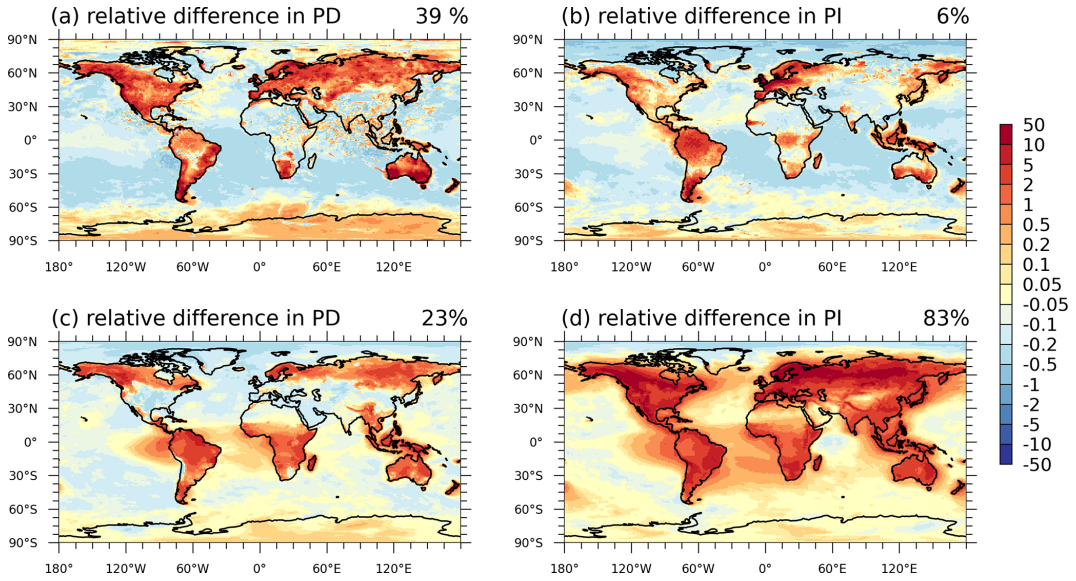

Figure 4. The relative change (unitless) of the simulated **(a, b)** vertically integrated nucleation rate ($j_{1.7\,\mathrm{nm}}$, below 15 km) and **(c, d)** vertical mean sub-20 nm growth rate after adding organic nucleation in PD and PI environments. Global mean values are shown on the top right of each figure.

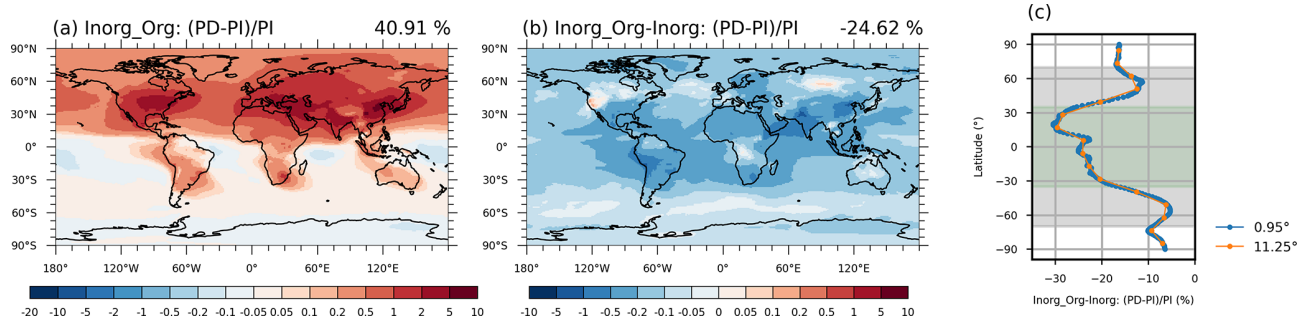

Figure 5. The global mean of the relative change in the vertically integrated CCN number at 0.2 % supersaturation in the PD experiment compared to the PI experiments after adding organic NPF mechanisms **(a)** and the difference of that value between cases with and without organic NPF **(b)**. The zonal mean of the information in **(b)** is shown in **(c)** (blue scatters show the zonal mean with an interval of 0.95°, and orange scatters show the zonal mean with an interval of 11.25°). The global average value is shown on the top right of each panel. Model experiments are described in Table 2, and model data come from the monthly mean value over 10 years.

icant reductions are transported to the western side of these regions, where most of the anthropogenic aerosol–cloud radiative forcing occurs, resulting in significant reductions in $\mathrm{ERF_{aci}}$ (Fig. 6b). The largest reduction of $\mathrm{ERF_{aci}}$ in the Southern Hemisphere (SH) occurs on the western side of the Amazon and Australia (Fig. 6b), where biogenic NPF causes the largest reduction in CCN concentrations from the PD to the PI experiment (Fig. 5a), driven by the large continental source of biogenic gases (Fig. S3). In some tropical oceanic regions of the SH, there are higher CCN concentrations in the PI atmosphere than in the PD atmosphere in Inorg_Org (Fig. 5a), caused by higher preindustrial ACCs (Fig. S3) and lower particle condensation sinks, leading to a positive $\mathrm{ERF_{aci}}$ (Fig. 6a). At mid-latitudes ($\sim$ 35–70°) in the NH, the reduction in $\mathrm{ERF_{aci}}$ is mainly caused by larger emissions of monoterpenes and, consequently, higher concentrations of HOMs in the PI environment of boreal forests in North America and Eurasia (Fig. S3). The large increase in sub-20 nm particle growth rate in the PI experiment resulting from HOM condensation also supports this point.

In previous studies (Zhu et al., 2019; Gordon et al., 2016), organic nucleation ($J_{\mathrm{Org,n}} + J_{\mathrm{Org,i}} + J_{\mathrm{SA\text{-}Org}}$) is the main reason for the higher CCN number in the PI simulation and thus leads to the reduction in $\mathrm{ERF_{aci}}$. However, in our simulation, the fractional change in total nucleation rate from PI to PD is larger after adding organic nucleation (1075 % in Inorg_Org and 796 % in Inorg) (Fig. 7). This is mainly caused by the heteromolecular nucleation rate of sulfuric acid and organics ($J_{\mathrm{SA\text{-}Org}}$), which is the dominant contributor to the total nucleation rate, showing greater increase in the PD experi-

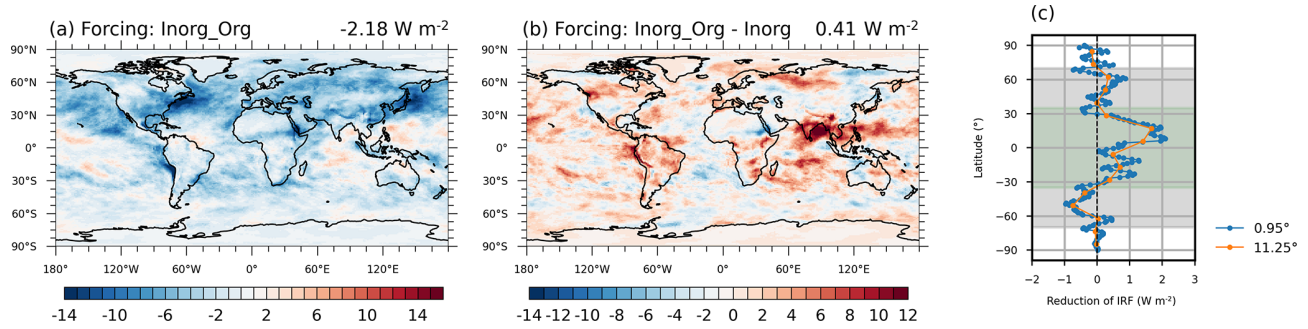

Figure 6. The effective radiative forcing due to aerosol–cloud interactions (ERF_{aci}) aerosol after including organic NPF **(a)** and the difference in the ERF_{aci} of anthropogenic aerosol between cases with and without organic NPF **(b)**. The zonal mean of the information in **(b)** is shown in **(c)** (blue scatters show the zonal mean with an interval of 0.95°, and orange scatters show the zonal mean with an interval of 11.25°). The global average value is shown on the top right of each panel. Model experiments are described in Table 2, and model data come from the monthly mean value over 10 years.

ment (Fig. S6) than in the PI experiment (Fig. S7). Especially in boreal forests, northern America, and Australia (Fig. S8), both H_2SO_4 and HOMs are abundant in the PD experiments (Figs. S2 and S3), leading to much larger $J_{SA\text{-}Org}$ values (Fig. S6). Therefore, the greater enhancement of CCN burden in the PI experiment and reduction in ERF_{aci} are likely caused by organic condensational growth on sub-20 nm particles (with PD fractional changes of 6 % in Inorg_Org and 58 % in Inorg; Fig. 7), instead of organic nucleation. Specifically, after incorporating the organic NPF mechanism, the growth rate of sub-20 nm particles increases more significantly in the PI experiment ($0.0083\,nm\,h^{-1}$) than in the PD experiment ($0.0036\,nm\,h^{-1}$) (Fig. 8). This is mainly due to the higher organic sub-20 nm growth rate in PI ($0.01\,nm\,h^{-1}$) compared to PD ($0.006\,nm\,h^{-1}$).

The most significant changes in ERF_{aci} reduction due to the inclusion of organic NPF are in tropical regions (Fig. 6c). This is different from previous studies (Zhu et al., 2019; Gordon et al., 2016), which showed that most of the reduction in ERF_{aci} occurs in the mid-latitudes of the NH, closely related to the distribution of HOM concentrations. Previous studies (Zhu et al., 2019; Gordon et al., 2016) did not account for organic nucleating species derived from isoprene oxidation, thereby neglecting ACC generation through self- and cross-reactions of isoprene- and monoterpene-derived radicals. Gordon et al. (2016) and Zhu et al. (2019) assumed that all organic nucleating species had the same volatility and can equally contribute to the organic nucleation. This simplification may have led to an overestimation of the organic nucleation rate and, consequently, the reduction in ERF_{aci} in the mid-latitudes. Our study highlights that only ACCs can contribute to pure organic nucleation due to their extremely low volatility. ACCs show high concentrations only in the Amazon, Central Africa, and Western Europe (Fig. S3), where the total nucleation rate is dominated by pure organic nucleation (Figs. S6 and S7). Furthermore, in these regions, there is the largest difference in ACC concentration between the PD and PI experiments (Fig. S3). Consequently, the most significant reductions in ERF_{aci} are in the Amazon, central Africa, Australia, and Southeast Asia (Fig. 6b), as well as the marine low-cloud regions to the west of these areas.

5 Summary and discussion

New particle formation (NPF) is widely recognised as an important source of atmospheric particles that significantly influence the Earth's climate. In the present work, the contribution of highly oxygenated organic molecules (HOMs) to cloud condensation nuclei (CCN) burden via organic nucleation is quantified in both present-day (PD) and preindustrial (PI) environments using a chemistry–climate model (Shao et al., 2024). The reduction in effective radiative forcing due to aerosol–cloud interactions (ERF_{aci}) caused by adding organic NPF mechanisms is also assessed.

After incorporating the organic NPF scheme with state-of-the-art chemical mechanisms for biogenic HOMs into CAM6-Chem, the simulated CCN numbers agree better with measurements across different backgrounds (including mountain, rural, and marine) (Fig. 1). Globally, the inclusion of organic-related NPF processes results in a 39 % increase in CCN burden in the PI experiment and an 18 % increase in the PD experiment. Similarly, cloud droplet number concentration (CDNC) at the top of low clouds in the Inorg_Org simulation rises by 12 % in the PI experiment but only by 7 % in the PD experiment. The greater enhancement of CCN burden in the PI experiment is primarily driven by organic condensational growth on sub-20 nm particles, rather than organic nucleation. We noted that previous studies (Zhu et al., 2019; Gordon et al., 2016) attributed the greater enhancement of CCN burden in the PI experiment to organic nucleation, which is likely due to an overestimation of the organic nucleation rate by assuming uniform volatility among all organic nucleating species. In our study, only accretion products generated through self- and cross-reactions of bio-

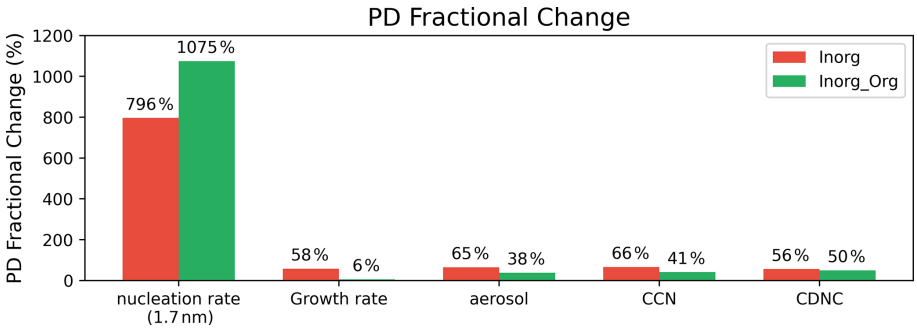

Figure 7. The global mean of the PD fractional change ((PD-PI)/PI) of key variables. Model experiments are described in Table 2, and model data come from the monthly mean value over 10 years.

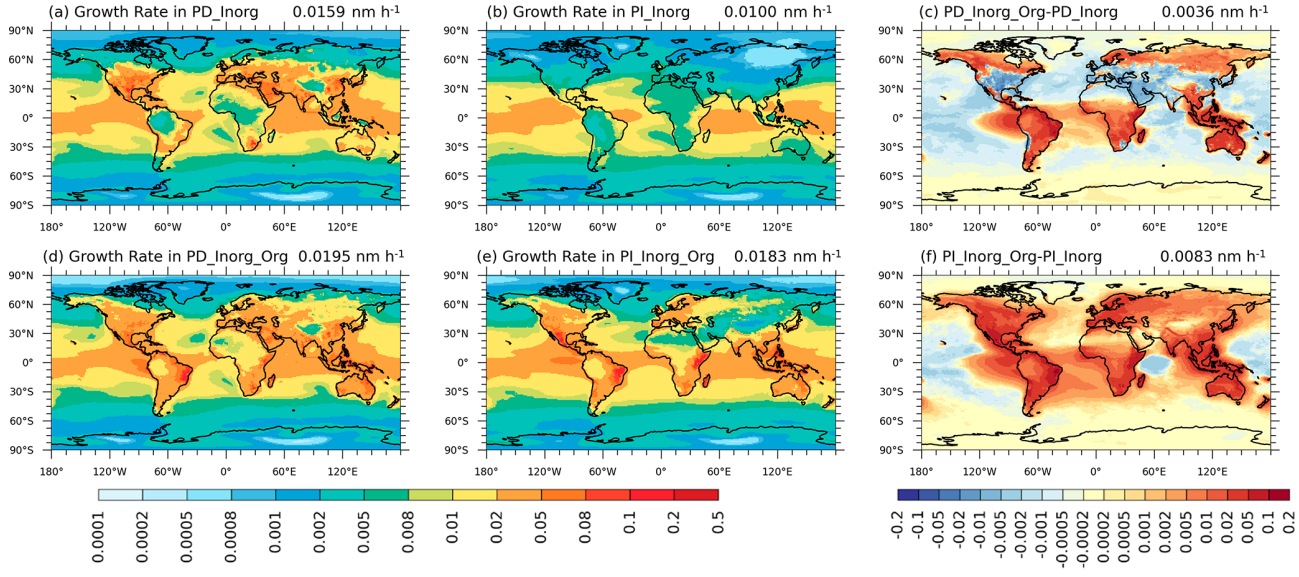

Figure 8. Spatial distribution of the simulated vertically mean growth rate in the **(a, d)** PD and **(b, e)** PI experiments. The difference between Inorg_Org and Inorg in the PD and PI experiments is shown in **(c)** and **(f)** (unit: $\mathrm{nm\,h^{-1}}$). Global mean values are shown on the top right of each figure.

genic radicals are allowed to contribute to pure organic nucleation, making heteromolecular nucleation ($J_{\mathrm{SA\text{-}Org}}$) the dominant nucleation pathway. Higher H_2SO_4 concentrations in the PD environment further enhance nucleation rates compared to the PI atmosphere. In contrast, HOM concentrations are higher in the PI atmosphere (Fig. S3), leading to a much greater condensation of organics on sub-20 nm particles in the PI experiments.

The larger increase in both CCN and CDNC in the PI environment directly leads to an increased aerosol indirect effect in the PI case, which is the baseline for calculating $\mathrm{ERF_{aci}}$ in the global model, thereby decreasing the cooling effect of $\mathrm{ERF_{aci}}$ ($\sim 0.42\,\mathrm{W\,m^{-2}}$, corresponding to 16 % of its original magnitude) (Fig. 6). The reduction in the magnitude of $\mathrm{ERF_{aci}}$ is primarily concentrated in boreal forests and low latitudes (Amazon, central Africa, and Southeast China), consistent with the greater increase in CCN and cloud droplet numbers in the PI atmosphere of those regions.

Although we improve the simulations of CCN numbers by utilising explicit chemical reactions to replace the traditional fixed yield method, further studies are needed to better align simulated HOM concentrations with widespread measurements. For instance, the autoxidation reaction step, which likely affects the volatility of the final products and their contribution to organic nucleation, has not yet been conclusively determined in chamber experiments (Roldin et al., 2019; Weber et al., 2020; Berndt et al., 2018). Also, the mechanisms used in this study cannot yet capture all variations in observed NPF events (Shao et al., 2024), especially in polluted environments. More lab-based studies are needed to examine the chemical reactions of anthropogenic HOMs to identify which ones could contribute to NPF mechanisms.

Code availability. Specific code developments and improvements in this study can be found in Shao et al. (2024). If further information is needed, please feel free to contact Xinyue Shao.

Data availability. The observational data of CCN number concentrations used in this study were obtained from ships, stations, and aircraft at various locations. All data are available for download at http://www.archive.arm.gov/discovery/#v/results/ (last access: 20 December 2025).

Supplement. The supplement related to this article is available online at https://doi.org/10.5194/acp-26-4439-2026-supplement.

Author contributions. MW and XD designed the study. XS performed the data analysis, produced the figures, and wrote the paper draft. LAR and MY collected the data and prepared the dataset. YL, SRA, WS, HW, JW, WZ, and KSC contributed to the analysis methods. DSJ provided the model. All the authors contributed to the discussion, writing, and editing of the paper.

Competing interests. At least one of the (co-)authors is a member of the editorial board of *Atmospheric Chemistry and Physics*. The peer-review process was guided by an independent editor, and the authors also have no other competing interests to declare.

Disclaimer. Publisher's note: Copernicus Publications remains neutral with regard to jurisdictional claims made in the text, published maps, institutional affiliations, or any other geographical representation in this paper. While Copernicus Publications makes every effort to include appropriate place names, the final responsibility lies with the authors. Views expressed in the text are those of the authors and do not necessarily reflect the views of the publisher.

Acknowledgements. We greatly thank the High Performance Computing Center (HPCC) of Nanjing University for providing the computational resources used in this work. We thank all the scientists, software engineers, and administrators, who contributed to the development of CESM2.

Financial support. This work is supported by the National Natural Science Foundation of China (grant nos. 2024YFC3711905, U2342223, and 91744208), and the Fundamental Research Funds for the Central Universities – CEMAC "GeoX" Interdisciplinary Program by the Frontiers Science Center for Critical Earth Material Cycling, Nanjing University. This work was also supported by the Postgraduate Research and Practice Innovation Program of Jiangsu Province (grant no. KYCX25_0220) and the Fundamental Research Funds for the Central Universities (grant no. 14380230).

Review statement. This paper was edited by Simone Tilmes and reviewed by three anonymous referees.

References

Albrecht, B. A.: Aerosols, Cloud Microphysics, and Fractional Cloudiness, Science, 245, 1227–1230, https://doi.org/10.1126/science.245.4923.1227, 1989.

Berndt, T., Mentler, B., Scholz, W., Fischer, L., Herrmann, H., Kulmala, M., and Hansel, A.: Accretion Product Formation from Ozonolysis and OH Radical Reaction of α-Pinene: Mechanistic Insight and the Influence of Isoprene and Ethylene, Environ. Sci. Technol., 52, 11069–11077, https://doi.org/10.1021/acs.est.8b02210, 2018.

Bianchi, F., Kurten, T., Riva, M., Mohr, C., Rissanen, M. P., Roldin, P., Berndt, T., Crounse, J. D., Wennberg, P. O., Mentel, T. F., Wildt, J., Junninen, H., Jokinen, T., Kulmala, M., Worsnop, D. R., Thornton, J. A., Donahue, N., Kjaergaard, H. G., and Ehn, M.: Highly Oxygenated Organic Molecules (HOM) from Gas-Phase Autoxidation Involving Peroxy Radicals: A Key Contributor to Atmospheric Aerosol, Chem. Rev., 119, 3472–3509, https://doi.org/10.1021/acs.chemrev.8b00395, 2019.

Bodhaine, B. A.: Aerosol measurements at four background sites, J. Geophys. Res.-Oceans, 88, 10753–10768, https://doi.org/10.1029/JC088iC15p10753, 1983.

Carslaw, K. S., Lee, L. A., Reddington, C. L., Pringle, K. J., Rap, A., Forster, P. M., Mann, G. W., Spracklen, D. V., Woodhouse, M. T., Regayre, L. A., and Pierce, J. R.: Large contribution of natural aerosols to uncertainty in indirect forcing, Nature, 503, 67–71, https://doi.org/10.1038/nature12674, 2013.

Dunne, E. M., Gordon, H., Kurten, A., Almeida, J., Duplissy, J., Williamson, C., Ortega, I. K., Pringle, K. J., Adamov, A., Baltensperger, U., Barmet, P., Benduhn, F., Bianchi, F., Breitenlechner, M., Clarke, A., Curtius, J., Dommen, J., Donahue, N. M., Ehrhart, S., Flagan, R. C., Franchin, A., Guida, R., Hakala, J., Hansel, A., Heinritzi, M., Jokinen, T., Kangasluoma, J., Kirkby, J., Kulmala, M., Kupc, A., Lawler, M. J., Lehtipalo, K., Makhmutov, V., Mann, G., Mathot, S., Merikanto, J., Miettinen, P., Nenes, A., Onnela, A., Rap, A., Reddington, C. L. S., Riccobono, F., Richards, N. A. D., Rissanen, M. P., Rondo, L., Sarnela, N., Schobesberger, S., Sengupta, K., Simon, M., Sipilaa, M., Smith, J. N., Stozkhov, Y., Tome, A., Trostl, J., Wagner, P. E., Wimmer, D., Winkler, P. M., Worsnop, D. R., and Carslaw, K. S.: Global atmospheric particle formation from CERN CLOUD measurements, Science, 354, 1119–1124, https://doi.org/10.1126/science.aaf2649, 2016.

Ehn, M., Thornton, J. A., Kleist, E., Sipila, M., Junninen, H., Pullinen, I., Springer, M., Rubach, F., Tillmann, R., Lee, B., Lopez-Hilfiker, F., Andres, S., Acir, I. H., Rissanen, M., Jokinen, T., Schobesberger, S., Kangasluoma, J., Kontkanen, J., Nieminen, T., Kurten, T., Nielsen, L. B., Jorgensen, S., Kjaergaard, H. G., Canagaratna, M., Dal Maso, M., Berndt, T., Petaja, T., Wahner, A., Kerminen, V. M., Kulmala, M., Worsnop, D. R., Wildt, J., and Mentel, T. F.: A large source of low-volatility secondary organic aerosol, Nature, 506, 476, https://doi.org/10.1038/nature13032, 2014.

Emmons, L. K., Schwantes, R. H., Orlando, J. J., Tyndall, G., Kinnison, D., Lamarque, J. F., Marsh, D., Mills, M. J., Tilmes, S.,

Bardeen, C., Buchholz, R. R., Conley, A., Gettelman, A., Garcia, R., Simpson, I., Blake, D. R., Meinardi, S., and Pétron, G.: The Chemistry Mechanism in the Community Earth System Model Version 2 (CESM2), J. Adv. Model. Earth Sy., 12, e2019MS001882, https://doi.org/10.1029/2019ms001882, 2020.

Ge, W., Liu, J., Yi, K., Xu, J., Zhang, Y., Hu, X., Ma, J., Wang, X., Wan, Y., Hu, J., Zhang, Z., Wang, X., and Tao, S.: Influence of atmospheric in-cloud aqueous-phase chemistry on the global simulation of SO_2 in CESM2, Atmos. Chem. Phys., 21, 16093–16120, https://doi.org/10.5194/acp-21-16093-2021, 2021.

Ge, W., Liu, J., Xiang, S., Zhou, Y., Zhou, J., Hu, X., Ma, J., Wang, X., Wan, Y., Hu, J., Zhang, Z., Wang, X., and Tao, S.: Improvement and Uncertainties of Global Simulation of Sulfate Concentration and Radiative Forcing in CESM2, J. Geophys. Res.-Atmos., 127, e2022JD037623, https://doi.org/10.1029/2022JD037623, 2022.

Ghan, S. J.: Technical Note: Estimating aerosol effects on cloud radiative forcing, Atmos. Chem. Phys., 13, 9971–9974, https://doi.org/10.5194/acp-13-9971-2013, 2013.

Gordon, H., Sengupta, K., Rap, A., Duplissy, J., Frege, C., Williamson, C., Heinritzi, M., Simon, M., Yan, C., Almeida, J., Trostl, J., Nieminen, T., Ortega, I. K., Wagner, R., Dunne, E. M., Adamov, A., Amorim, A., Bernhammer, A. K., Bianchi, F., Breitenlechner, M., Brilke, S., Chen, X. M., Craven, J. S., Dias, A., Ehrhart, S., Fischer, L., Flagan, R. C., Franchin, A., Fuchs, C., Guida, R., Hakala, J., Hoyle, C. R., Jokinen, T., Junninen, H., Kangasluoma, J., Kim, J., Kirkby, J., Krapf, M., Kurten, A., Laaksonen, A., Lehtipalo, K., Makhmutov, V., Mathot, S., Molteni, U., Monks, S. A., Onnela, A., Perakyla, O., Piel, F., Petaja, T., Praplanh, A. P., Pringle, K. J., Richards, N. A. D., Rissanen, M. P., Rondo, L., Sarnela, N., Schobesberger, S., Scott, C. E., Seinfeldo, J. H., Sharma, S., Sipila, M., Steiner, G., Stozhkov, Y., Stratmann, F., Tome, A., Virtanen, A., Vogel, A. L., Wagner, A. C., Wagner, P. E., Weingartner, E., Wimmer, D., Winkler, P. M., Ye, P. L., Zhang, X., Hansel, A., Dommen, J., Donahue, N. M., Worsnop, D. R., Baltensperger, U., Kulmala, M., Curtius, J., and Carslaw, K. S.: Reduced anthropogenic aerosol radiative forcing caused by biogenic new particle formation, P. Natl. Acad. Sci. USA, 113, 12053–12058, https://doi.org/10.1073/pnas.1602360113, 2016.

Gordon, H., Kirkby, J., Baltensperger, U., Bianchi, F., Breitenlechner, M., Curtius, J., Dias, A., Dommen, J., Donahue, N. M., Dunne, E. M., Duplissy, J., Ehrhart, S., Flagan, R. C., Frege, C., Fuchs, C., Hansel, A., Hoyle, C. R., Kulmala, M., Kurten, A., Lehtipalo, K., Makhmutov, V., Molteni, U., Rissanen, M. P., Stozkhov, Y., Trostl, J., Tsagkogeorgas, G., Wagner, R., Williamson, C., Wimmer, D., Winkler, P. M., Yan, C., and Carslaw, K. S.: Causes and importance of new particle formation in the present-day and preindustrial atmospheres, J. Geophys. Res.-Atmos., 122, 8739–8760, https://doi.org/10.1002/2017jd026844, 2017.

Guenther, A. B., Jiang, X., Heald, C. L., Sakulyanontvittaya, T., Duhl, T., Emmons, L. K., and Wang, X.: The Model of Emissions of Gases and Aerosols from Nature version 2.1 (MEGAN2.1): an extended and updated framework for modeling biogenic emissions, Geosci. Model Dev., 5, 1471–1492, https://doi.org/10.5194/gmd-5-1471-2012, 2012.

He, J. and Zhang, Y.: Improvement and further development in CESM/CAM5: gas-phase chemistry and inorganic aerosol treatments, Atmos. Chem. Phys., 14, 9171–9200, https://doi.org/10.5194/acp-14-9171-2014, 2014.

He, J., Zhang, Y., Glotfelty, T., He, R., Bennartz, R., Rausch, J., and Sartelet, K.: Decadal simulation and comprehensive evaluation of CESM/CAM5.1 with advanced chemistry, aerosol microphysics, and aerosol-cloud interactions, J. Adv. Model. Earth Sy., 7, 110–141, https://doi.org/10.1002/2014MS000360, 2015.

Hoesly, R. M., Smith, S. J., Feng, L., Klimont, Z., Janssens-Maenhout, G., Pitkanen, T., Seibert, J. J., Vu, L., Andres, R. J., Bolt, R. M., Bond, T. C., Dawidowski, L., Kholod, N., Kurokawa, J.-I., Li, M., Liu, L., Lu, Z., Moura, M. C. P., O'Rourke, P. R., and Zhang, Q.: Historical (1750–2014) anthropogenic emissions of reactive gases and aerosols from the Community Emissions Data System (CEDS), Geosci. Model Dev., 11, 369–408, https://doi.org/10.5194/gmd-11-369-2018, 2018.

Jefferson, A.: Empirical estimates of CCN from aerosol optical properties at four remote sites, Atmos. Chem. Phys., 10, 6855–6861, https://doi.org/10.5194/acp-10-6855-2010, 2010.

Jokinen, T., Berndt, T., Makkonen, R., Kerminen, V. M., Junninen, H., Paasonen, P., Stratmann, F., Herrmann, H., Guenther, A. B., Worsnop, D. R., Kulmala, M., Ehn, M., and Sipila, M.: Production of extremely low volatile organic compounds from biogenic emissions: Measured yields and atmospheric implications, P. Natl. Acad. Sci. USA, 112, 7123–7128, https://doi.org/10.1073/pnas.1423977112, 2015.

Kazil, J., Stier, P., Zhang, K., Quaas, J., Kinne, S., O'Donnell, D., Rast, S., Esch, M., Ferrachat, S., Lohmann, U., and Feichter, J.: Aerosol nucleation and its role for clouds and Earth's radiative forcing in the aerosol-climate model ECHAM5-HAM, Atmos. Chem. Phys., 10, 10733–10752, https://doi.org/10.5194/acp-10-10733-2010, 2010.

Kirkby, J., Duplissy, J., Sengupta, K., Frege, C., Gordon, H., Williamson, C., Heinritzi, M., Simon, M., Yan, C., Almeida, J., Trostl, J., Nieminen, T., Ortega, I. K., Wagner, R., Adamov, A., Amorim, A., Bernhammer, A. K., Bianchi, F., Breitenlechner, M., Brilke, S., Chen, X. M., Craven, J., Dias, A., Ehrhart, S., Flagan, R. C., Franchin, A., Fuchs, C., Guida, R., Hakala, J., Hoyle, C. R., Jokinen, T., Junninen, H., Kangasluoma, J., Kim, J., Krapf, M., Kurten, A., Laaksonen, A., Lehtipalo, K., Makhmutov, V., Mathot, S., Molteni, U., Onnela, A., Perakyla, O., Piel, F., Petaja, T., Praplan, A. P., Pringle, K., Rap, A., Richards, N. A. D., Riipinen, I., Rissanen, M. P., Rondo, L., Sarnela, N., Schobesberger, S., Scott, C. E., Seinfeld, J. H., Sipila, M., Steiner, G., Stozhkov, Y., Stratmann, F., Tome, A., Virtanen, A., Vogel, A. L., Wagner, A. C., Wagner, P. E., Weingartner, E., Wimmer, D., Winkler, P. M., Ye, P. L., Zhang, X., Hansel, A., Dommen, J., Donahue, N. M., Worsnop, D. R., Baltensperger, U., Kulmala, M., Carslaw, K. S., and Curtius, J.: Ion-induced nucleation of pure biogenic particles, Nature, 533, 521, https://doi.org/10.1038/nature17953, 2016.

Kooperman, G. J., Pritchard, M. S., Ghan, S. J., Wang, M., Somerville, R. C. J., and Russell, L. M.: Constraining the influence of natural variability to improve estimates of global aerosol indirect effects in a nudged version of the Community Atmosphere Model 5, J. Geophys. Res.-Atmos., 117, https://doi.org/10.1029/2012jd018588, 2012.

Kulmala, M., Lehtinen, K. E. J., and Laaksonen, A.: Cluster activation theory as an explanation of the linear dependence between formation rate of 3nm particles and sulphuric acid concentration,

Atmos. Chem. Phys., 6, 787–793, https://doi.org/10.5194/acp-6-787-2006, 2006.

Lee, S.-H., Gordon, H., Yu, H., Lehtipalo, K., Haley, R., Li, Y., and Zhang, R.: New Particle Formation in the Atmosphere: From Molecular Clusters to Global Climate, J. Geophys. Res.-Atmos., 124, 7098–7146, https://doi.org/10.1029/2018JD029356, 2019.

Li, M., Liu, H., Geng, G., Hong, C., Liu, F., Song, Y., Tong, D., Zheng, B., Cui, H., Man, H., Zhang, Q., and He, K.: Anthropogenic emission inventories in China: a review, National Science Review, 4, 834–866, https://doi.org/10.1093/nsr/nwx150, 2017.

Liu, X., Ma, P.-L., Wang, H., Tilmes, S., Singh, B., Easter, R. C., Ghan, S. J., and Rasch, P. J.: Description and evaluation of a new four-mode version of the Modal Aerosol Module (MAM4) within version 5.3 of the Community Atmosphere Model, Geosci. Model Dev., 9, 505–522, https://doi.org/10.5194/gmd-9-505-2016, 2016.

Merikanto, J., Napari, I., Vehkamaki, H., Anttila, T., and Kulmala, M.: New parameterization of sulfuric acid-ammonia-water ternary nucleation rates at tropospheric conditions, J. Geophys. Res.-Atmos., 112, https://doi.org/10.1029/2006jd007977, 2007.

Merikanto, J., Spracklen, D. V., Mann, G. W., Pickering, S. J., and Carslaw, K. S.: Impact of nucleation on global CCN, Atmos. Chem. Phys., 9, 8601–8616, https://doi.org/10.5194/acp-9-8601-2009, 2009.

O'Neill, B. C., Kriegler, E., Ebi, K. L., Kemp-Benedict, E., Riahi, K., Rothman, D. S., van Ruijven, B. J., van Vuuren, D. P., Birkmann, J., Kok, K., Levy, M., and Solecki, W.: The roads ahead: Narratives for shared socioeconomic pathways describing world futures in the 21st century, Global Environ. Change, 42, 169–180, https://doi.org/10.1016/j.gloenvcha.2015.01.004, 2017.

Peace, A. H., Carslaw, K. S., Lee, L. A., Regayre, L. A., Booth, B. B. B., Johnson, J. S., and Bernie, D.: Effect of aerosol radiative forcing uncertainty on projected exceedance year of a 1.5 °C global temperature rise, Environ. Res. Lett., 15, 0940a0946, https://doi.org/10.1088/1748-9326/aba20c, 2020.

Pierce, J. R. and Adams, P. J.: A Computationally Efficient Aerosol Nucleation/Condensation Method: PseudoSteady-State Sulfuric Acid, Aerosol Sci. Technol., 43, 216–226, https://doi.org/10.1080/02786820802587896, 2009.

Reddington, C. L., Carslaw, K. S., Stier, P., Schutgens, N., Coe, H., Liu, D., Allan, J., Browse, J., Pringle, K. J., Lee, L. A., Yoshioka, M., Johnson, J. S., Regayre, L. A., Spracklen, D. V., Mann, G. W., Clarke, A., Hermann, M., Henning, S., Wex, H., Kristensen, T. B., Leaitch, W. R., Pöschl, U., Rose, D., Andreae, M. O., Schmale, J., Kondo, Y., Oshima, N., Schwarz, J. P., Nenes, A., Anderson, B., Roberts, G. C., Snider, J. R., Leck, C., Quinn, P. K., Chi, X., Ding, A., Jimenez, J. L., and Zhang, Q.: The Global Aerosol Synthesis and Science Project (GASSP): Measurements and Modeling to Reduce Uncertainty, B. Am. Meteorol. Soc., 98, 1857–1877, https://doi.org/10.1175/bams-d-15-00317.1, 2017.

Riccobono, F., Schobesberger, S., Scott, C. E., Dommen, J., Ortega, I. K., Rondo, L., Almeida, J., Amorim, A., Bianchi, F., Breitenlechner, M., David, A., Downard, A., Dunne, E. M., Duplissy, J., Ehrhart, S., Flagan, R. C., Franchin, A., Hansel, A., Junninen, H., Kajos, M., Keskinen, H., Kupc, A., Kurten, A., Kvashin, A. N., Laaksonen, A., Lehtipalo, K., Makhmutov, V., Mathot, S., Nieminen, T., Onnela, A., Petaja, T., Praplan, A. P., Santos, F. D., Schallhart, S., Seinfeld, J. H., Sipila, M., Spracklen, D. V., Stozhkov, Y., Stratmann, F., Tome, A., Tsagkogeorgas, G., Vaattovaara, P., Viisanen, Y., Vrtala, A., Wagner, P. E., Weingartner, E., Wex, H., Wimmer, D., Carslaw, K. S., Curtius, J., Donahue, N. M., Kirkby, J., Kulmala, M., Worsnop, D. R., and Baltensperger, U.: Oxidation Products of Biogenic Emissions Contribute to Nucleation of Atmospheric Particles, Science, 344, 717–721, https://doi.org/10.1126/science.1243527, 2014.

Roldin, P., Ehn, M., Kurtén, T., Olenius, T., Rissanen, M. P., Sarnela, N., Elm, J., Rantala, P., Hao, L., Hyttinen, N., Heikkinen, L., Worsnop, D. R., Pichelstorfer, L., Xavier, C., Clusius, P., Öström, E., Petäjä, T., Kulmala, M., Vehkamäki, H., Virtanen, A., Riipinen, I., and Boy, M.: The role of highly oxygenated organic molecules in the Boreal aerosol-cloud-climate system, Nat. Commun., 10, 4370, https://doi.org/10.1038/s41467-019-12338-8, 2019.

Rosenfeld, D. and Lensky, I. M.: Satellite-Based Insights into Precipitation Formation Processes in Continental and Maritime Convective Clouds, B. Am. Meteorol. Soc., 79, 2457–2476, https://doi.org/10.1175/1520-0477(1998)079<2457:SBIIPF>2.0.CO;2, 1998.

Rosenfeld, D. and Woodley, W. L.: Deep convective clouds with sustained supercooled liquid water down to −37.5 °C, Nature, 405, 440–442, https://doi.org/10.1038/35013030, 2000.

Schwantes, R. H., Emmons, L. K., Orlando, J. J., Barth, M. C., Tyndall, G. S., Hall, S. R., Ullmann, K., St. Clair, J. M., Blake, D. R., Wisthaler, A., and Bui, T. P. V.: Comprehensive isoprene and terpene gas-phase chemistry improves simulated surface ozone in the southeastern US, Atmos. Chem. Phys., 20, 3739–3776, https://doi.org/10.5194/acp-20-3739-2020, 2020.

Seinfeld, J. H., Bretherton, C., Carslaw, K. S., Coe, H., DeMott, P. J., Dunlea, E. J., Feingold, G., Ghan, S., Guenther, A. B., Kahn, R., Kraucunas, I., Kreidenweis, S. M., Molina, M. J., Nenes, A., Penner, J. E., Prather, K. A., Ramanathan, V., Ramaswamy, V., Rasch, P. J., Ravishankara, A. R., Rosenfeld, D., Stephens, G., and Wood, R.: Improving our fundamental understanding of the role of aerosol–cloud interactions in the climate system, P. Natl. Acad. Sci. USA, 113, 5781–5790, https://doi.org/10.1073/pnas.1514043113, 2016.

Shao, X., Wang, M., Dong, X., Liu, Y., Shen, W., Arnold, S. R., Regayre, L. A., Andreae, M. O., Pöhlker, M. L., Jo, D. S., Yue, M., and Carslaw, K. S.: Global modeling of aerosol nucleation with a semi-explicit chemical mechanism for highly oxygenated organic molecules (HOMs), Atmos. Chem. Phys., 24, 11365–11389, https://doi.org/10.5194/acp-24-11365-2024, 2024.

Sihto, S.-L., Kulmala, M., Kerminen, V.-M., Dal Maso, M., Petäjä, T., Riipinen, I., Korhonen, H., Arnold, F., Janson, R., Boy, M., Laaksonen, A., and Lehtinen, K. E. J.: Atmospheric sulphuric acid and aerosol formation: implications from atmospheric measurements for nucleation and early growth mechanisms, Atmos. Chem. Phys., 6, 4079–4091, https://doi.org/10.5194/acp-6-4079-2006, 2006.

Spracklen, D. V., Carslaw, K. S., Kulmala, M., Kerminen, V. M., Sihto, S. L., Riipinen, I., Merikanto, J., Mann, G. W., Chipperfield, M. P., Wiedensohler, A., Birmili, W., and Lihavainen, H.: Contribution of particle formation to global cloud condensation nuclei concentrations, Geophys. Res. Lett., 35, https://doi.org/10.1029/2007gl033038, 2008.

Twomey, S.: The Influence of Pollution on the Shortwave Albedo of Clouds, J. Atmos. Sci.,

34, 1149–1152, https://doi.org/10.1175/1520-0469(1977)034<1149:TIOPOT>2.0.CO;2, 1977.

Uin, J., Aiken, A. C., Dubey, M. K., Kuang, C., Pekour, M., Salwen, C., Sedlacek, A. J., Senum, G., Smith, S., Wang, J., Watson, T. B., and Springston, S. R.: Atmospheric Radiation Measurement (ARM) Aerosol Observing Systems (AOS) for Surface-Based In Situ Atmospheric Aerosol and Trace Gas Measurements, J. Atmos. Ocean. Tech., 36, 2429–2447, https://doi.org/10.1175/JTECH-D-19-0077.1, 2019.

van Marle, M. J. E., Kloster, S., Magi, B. I., Marlon, J. R., Daniau, A.-L., Field, R. D., Arneth, A., Forrest, M., Hantson, S., Kehrwald, N. M., Knorr, W., Lasslop, G., Li, F., Mangeon, S., Yue, C., Kaiser, J. W., and van der Werf, G. R.: Historic global biomass burning emissions for CMIP6 (BB4CMIP) based on merging satellite observations with proxies and fire models (1750–2015), Geosci. Model Dev., 10, 3329–3357, https://doi.org/10.5194/gmd-10-3329-2017, 2017.

Vehkamaki, H., Kulmala, M., Napari, I., Lehtinen, K. E. J., Timmreck, C., Noppel, M., and Laaksonen, A.: An improved parameterization for sulfuric acid-water nucleation rates for tropospheric and stratospheric conditions, J. Geophys. Res.-Atmos., 107, AAC 3-1–AAC 3-10, https://doi.org/10.1029/2002jd002184, 2002.

Wang, J., Wood, R., Jensen, M. P., Chiu, J. C., Liu, Y., Lamer, K., Desai, N., Giangrande, S. E., Knopf, D. A., Kollias, P., Laskin, A., Liu, X., Lu, C., Mechem, D., Mei, F., Starzec, M., Tomlinson, J., Wang, Y., Yum, S. S., Zheng, G., Aiken, A. C., Azevedo, E. B., Blanchard, Y., China, S., Dong, X., Gallo, F., Gao, S., Ghate, V. P., Glienke, S., Goldberger, L., Hardin, J. C., Kuang, C., Luke, E. P., Matthews, A. A., Miller, M. A., Moffet, R., Pekour, M., Schmid, B., Sedlacek, A. J., Shaw, R. A., Shilling, J. E., Sullivan, A., Suski, K., Veghte, D. P., Weber, R., Wyant, M., Yeom, J., Zawadowicz, M., and Zhang, Z.: Aerosol and Cloud Experiments in the Eastern North Atlantic (ACE-ENA), B. Am. Meteorol. Soc., 103, E619–E641, https://doi.org/10.1175/BAMS-D-19-0220.1, 2022.

Wang, M. and Penner, J. E.: Aerosol indirect forcing in a global model with particle nucleation, Atmos. Chem. Phys., 9, 239–260, https://doi.org/10.5194/acp-9-239-2009, 2009.

Wang, X., Gordon, H., Grosvenor, D. P., Andreae, M. O., and Carslaw, K. S.: Contribution of regional aerosol nucleation to low-level CCN in an Amazonian deep convective environment: results from a regionally nested global model, Atmos. Chem. Phys., 23, 4431–4461, https://doi.org/10.5194/acp-23-4431-2023, 2023.

Watson-Parris, D. and Smith, C. J.: Large uncertainty in future warming due to aerosol forcing, Nat. Clim. Chang., 12, 1111–1113, https://doi.org/10.1038/s41558-022-01516-0, 2022.

Weber, J., Archer-Nicholls, S., Griffiths, P., Berndt, T., Jenkin, M., Gordon, H., Knote, C., and Archibald, A. T.: CRI-HOM: A novel chemical mechanism for simulating highly oxygenated organic molecules (HOMs) in global chemistry–aerosol–climate models, Atmos. Chem. Phys., 20, 10889–10910, https://doi.org/10.5194/acp-20-10889-2020, 2020.

Williamson, C. J., Kupc, A., Axisa, D., Bilsback, K. R., Bui, T., Campuzano-Jost, P., Dollner, M., Froyd, K. D., Hodshire, A. L., Jimenez, J. L., Kodros, J. K., Luo, G., Murphy, D. M., Nault, B. A., Ray, E. A., Weinzierl, B., Wilson, J. C., Yu, F., Yu, P., Pierce, J. R., and Brock, C. A.: A large source of cloud condensation nuclei from new particle formation in the tropics, Nature, 574, 399–403, https://doi.org/10.1038/s41586-019-1638-9, 2019.

Wood, R., Wyant, M., Bretherton, C. S., Rémillard, J., Kollias, P., Fletcher, J., Stemmler, J., de Szoeke, S., Yuter, S., Miller, M., Mechem, D., Tselioudis, G., Chiu, J. C., Mann, J. A. L., O'Connor, E. J., Hogan, R. J., Dong, X., Miller, M., Ghate, V., Jefferson, A., Min, Q., Minnis, P., Palikonda, R., Albrecht, B., Luke, E., Hannay, C., and Lin, Y.: Clouds, Aerosols, and Precipitation in the Marine Boundary Layer: An Arm Mobile Facility Deployment, B. Am. Meteorol. Soc., 96, 419–440, https://doi.org/10.1175/BAMS-D-13-00180.1, 2015.

Xu, R., Thornton, J. A., Lee, B. H., Zhang, Y., Jaeglé, L., Lopez-Hilfiker, F. D., Rantala, P., and Petäjä, T.: Global simulations of monoterpene-derived peroxy radical fates and the distributions of highly oxygenated organic molecules (HOMs) and accretion products, Atmos. Chem. Phys., 22, 5477–5494, https://doi.org/10.5194/acp-22-5477-2022, 2022.

Yu, F., Luo, G., Liu, X., Easter, R. C., Ma, X., and Ghan, S. J.: Indirect radiative forcing by ion-mediated nucleation of aerosol, Atmos. Chem. Phys., 12, 11451–11463, https://doi.org/10.5194/acp-12-11451-2012, 2012.

Yue, M., Dong, X., Wang, M., Emmons, L. K., Liang, Y., Tong, D., Liu, Y., and Liu, Y.: Modeling the Air Pollution and Aerosol-PBL Interactions Over China Using a Variable-Resolution Global Model, J. Geophys. Res.-Atmos., 128, e2023JD039130, https://doi.org/10.1029/2023jd039130, 2023.

Zhao, B., Shrivastava, M., Donahue, N. M., Gordon, H., Schervish, M., Shilling, J. E., Zaveri, R. A., Wang, J., Andreae, M. O., Zhao, C., Gaudet, B., Liu, Y., Fan, J., and Fast, J. D.: High concentration of ultrafine particles in the Amazon free troposphere produced by organic new particle formation, P. Natl. Acad. Sci. USA, 117, 25344–25351, https://doi.org/10.1073/pnas.2006716117, 2020.

Zhao, B., Fast, J., Shrivastava, M., Donahue, N. M., Gao, Y., Shilling, J. E., Liu, Y., Zaveri, R. A., Gaudet, B., Wang, S., Wang, J., Li, Z., and Fan, J.: Formation Process of Particles and Cloud Condensation Nuclei Over the Amazon Rainforest: The Role of Local and Remote New-Particle Formation, Geophys. Res. Lett., 49, e2022GL100940, https://doi.org/10.1029/2022GL100940, 2022.

Zheng, G., Sedlacek, A. J., Aiken, A. C., Feng, Y., Watson, T. B., Raveh-Rubin, S., Uin, J., Lewis, E. R., and Wang, J.: Long-range transported North American wildfire aerosols observed in marine boundary layer of eastern North Atlantic, Environ. Int., 139, 105680, https://doi.org/10.1016/j.envint.2020.105680, 2020.

Zhu, J., Penner, J. E., Yu, F., Sillman, S., Andreae, M. O., and Coe, H.: Decrease in radiative forcing by organic aerosol nucleation, climate, and land use change, Nat. Commun., 10, 423, https://doi.org/10.1038/s41467-019-08407-7, 2019.